Numerical Investigations to Suppress Thermal Deformation of the Large Deployable Reflector during Earth Eclipse in Space

Kaori Shoji [1], Motofumi Usui [2] and Daigoro Isobe [3]

[1] *University of Tsukuba, Tennodai 1-1-1, Tsukuba-shi, Ibaraki, JAPAN*
[2] *Japan Aerospace Exploration Agency, Higashi-machi Jindaiji 7-44-1, Chofu-shi, Tokyo, JAPAN*
[3] *University of Tsukuba, Tennodai 1-1-1, Tsukuba-shi, Ibaraki, JAPAN*

Abstract

Space structures encounter various severe environments in space. One of these environments is severe thermal conditions. The signal level of the radio wave from the large deployable reflector (LDR) mounted on the Engineering Test Satellite -VIII (ETS-VIII) was observed to change during an Earth eclipse. This phenomenon was assumed to be caused by the thermal deformation of the LDR. Therefore, in this study, a means to suppress the thermal deformation is proposed and demonstrated by focusing on the internal force generated at the springs used to deploy the antenna. According to the numerical results obtained from finite element analyses, the thermal deformations at all apices that support the reflectors were suppressed at a high correction rate by adjusting the coefficients of thermal expansion in the structural members and by controlling spring forces differently in four areas depending on the distances from the constraint point.

Keywords: ETS-VIII, finite element analysis, large deployable reflector, large space structure, thermal deformation, earth eclipse, communication beam, communications satellite.

Introduction

Space structures encounter various severe environments in space. One of these environments is severe thermal conditions. When the Engineering Test Satellite -VIII (ETS-VIII) entered the Earth's shadow, the difference in the temperature during the day time and night time was approximately 200°C [1], as shown in Fig. 1. During this eclipse time, the signal level of a radio wave from the large deployable reflector (LDR) mounted on the ETS-VIII was observed to change [2]. According to previous work [1], the midpoint of the LDR was confirmed to deform by approximately 5 mm as the temperature decreased, which led to a 50- to 60-km transition on the surface of the earth. This phenomenon was assumed to be caused by the thermal deformation of the LDR [3]. It

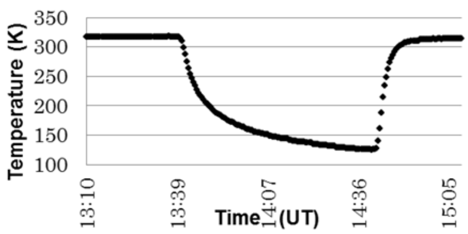

Fig. 1: Temperature of the LDR during Earth eclipse

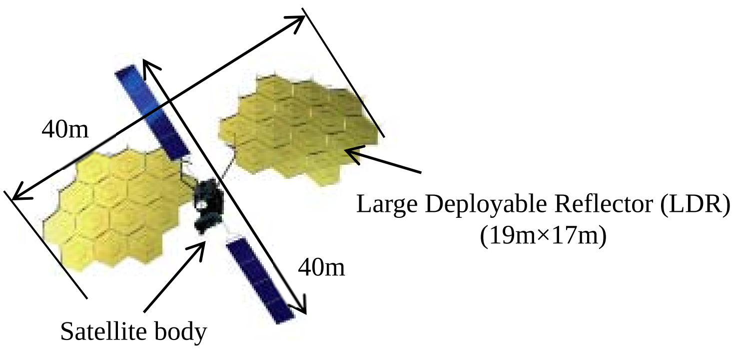

Fig. 2: ETS-VIII (Launched in 2006)

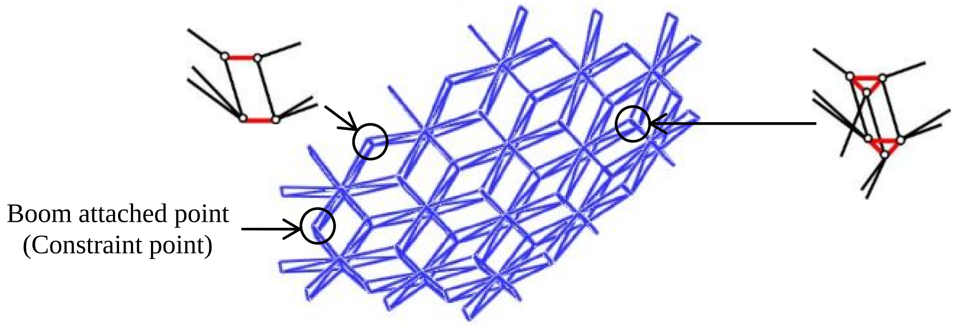

Fig. 3: 14-module model for analysis and the structural connections of the model

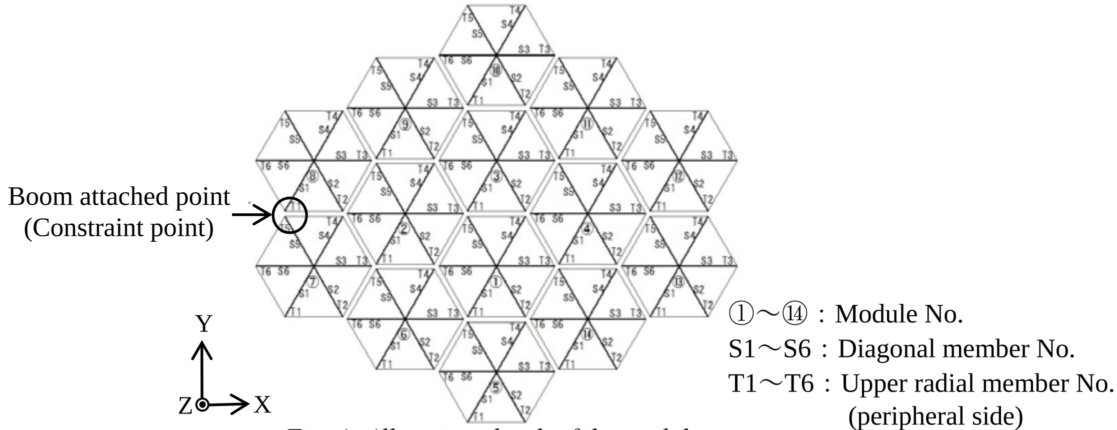

Fig. 4: Allocation sketch of the modules

was not a critical issue for the ETS-VIII because the communication beam from the LDR tended to spread over a wide range. However, it may affect the performance of such satellites in the future where highly accurate pinpoint communication beams are expected to be required.

In this paper, we constructed a finite element model of the LDR and performed a thermal deformation analysis to investigate the behaviour of the LDR during thermal transition. Furthermore, we sought a means to suppress the thermal deformation mechanically by focusing on the internal force generated by the spring used to deploy the antenna and by optimizing the coefficient of thermal expansion of the constituent members.

Numerical Model of the LDR

In 2006, the Japan Aerospace Exploration Agency (JAXA) launched the ETS-VIII into a geostationary satellite orbit. Figure 2 shows a general sketch of the ETS-VIII. There are two LDRs, which are the largest antennas mounted on the satellite. Each LDR is as large as a tennis court. This parabolic antenna consists of 14 hexagonal modules and is highly extendable because these modules are all identical and connected with pin joints to reduce mechanical interaction.

In this study, a 14-module model of the LDR was constructed for analysis. Figure 3 shows the 14-module model and the structural connections of the model. The mechanical interaction was minimized because of these pin joints. Two structural members, one each from two modules, are constrained perfectly to the boom. The boom is connected perfectly with the satellite body. Figure 4 shows the allocation sketch of the 14 modules.

Figure 5 shows an overview of one module. The LDR consists of CFRP tubes and titanium alloy joints. Figure 6 shows a structural drawing of the deployable mechanism. The spring used to deploy the antenna is installed at the centre axis member in all modules. The designed residual spring force after completion of antenna deployment is 233 N. The members are referred to as the upper radial member, the lower radial member, the diagonal member, the centre axis member and the longitudinal member. An automatic open umbrella mechanism consisting of a spring element and a stretcher element, as shown in Fig. 7, is introduced into the numerical model. Consequently, an internal force is transmitted through the stretcher element to the diagonal member by applying the spring force.

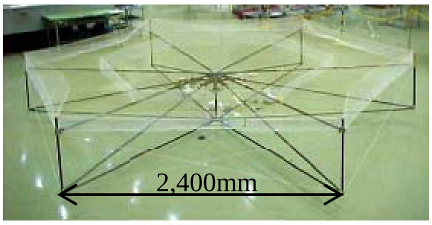

Fig. 5: Overview of one module

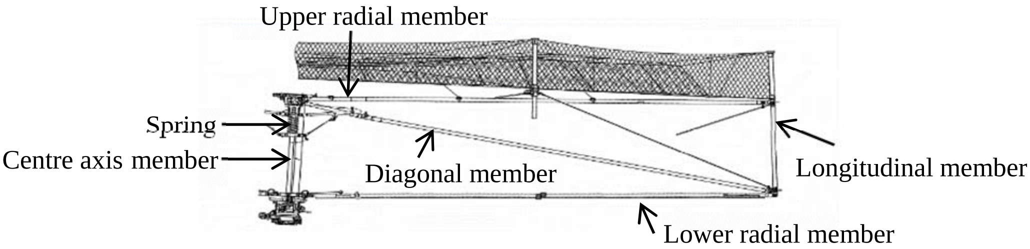

Fig. 6: Structural drawing of a deployable mechanism

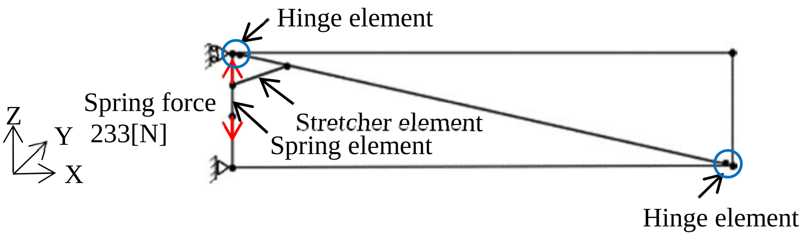

Fig. 7: Modelling of an automatic open umbrella mechanism

Thermal Expansion Properties of Constituent Members

Combined coefficient of thermal expansion (Combined CTE)

The combined coefficient of thermal expansion (Combined CTE) was calculated from the constituent ratio of CFRP and titanium alloy components, as shown in the following equation.

$$\alpha_C = \frac{l_{CFRP}}{L} \times \alpha_{CFRP} + \frac{l_{Titanium}}{L} \times \alpha_{Titanium} \tag{1}$$

where L is the total length, l_{CFRP} is the length of CFRP, α_{CFRP} is the CTE of CFRP, $l_{Titanium}$ is the length of titanium and $\alpha_{Titanium}$ is the CTE of titanium.

Table 1 shows the dimensions and material properties of the constituent members. The combined CTEs vary because of differences in the fibre orientation angle of each member and in the ratio of titanium alloy components to the total length of the member. Moreover, the upper radial members expand, whereas other members shrink as the temperature decreases. This indicates that the structure of the LDR is expected to have complex behaviour during the temperature transition.

Thermal strain

The thermal expansion is considered using the following equation, which expresses the relation between the temperature of an object and the thermal strain:

$$\Delta\varepsilon_T = \alpha\Delta T \tag{2}$$

where $\Delta\varepsilon_T$ is the thermal strain increment, α is the coefficient of thermal expansion, and ΔT is the temperature increment. The relation between the mechanical strain and the thermal strain can be expressed as the following equation.

Table 1: Dimensions and material properties of constituent members

	Material	CFRP laminate (degree)	Dimensions (mm)	CTE of CFRP (10-6/K)	Combined CTE (10-6/K)
Upper radial member	CFRP	(0/15/90/-15/0)	22×0.4×2305	- 1.07	- 0.182
Lower radial member	CFRP	(0/15/90/-15/0)	20×0.4×2328	- 1.07	0.312
Diagonal member	CFRP	(0/15/90/-15/0)	20×0.4×2308	- 0.33	0.948
Centre axis member	CFRP	(0,90)/(±45)/(0,90)/(±45)/(0,90)	20×1×573	2.97	3.49
Longitudinal member	CFRP	(0/15/90/-15/0/0)	20×0.48×554	- 1.11	0.277
Joint member	Titanium alloy	-	-	-	8.8

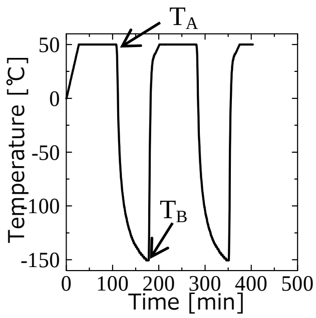

Fig. 8: Applied thermal history

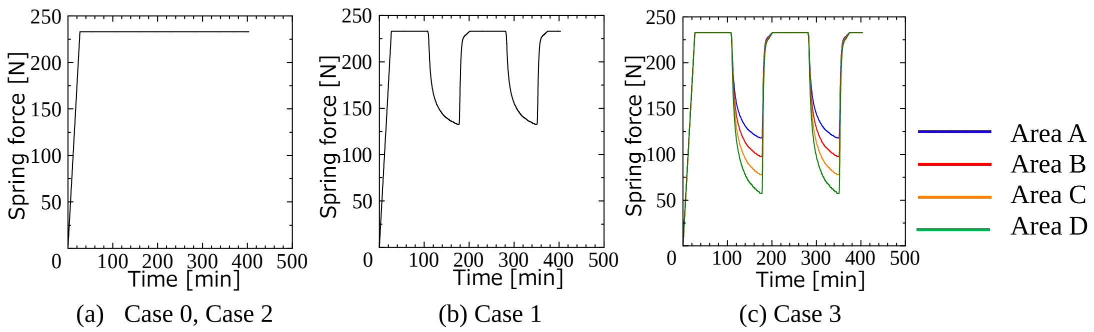

Fig. 9: Applied spring force histories

$$\varepsilon_m = \varepsilon - \varepsilon_T \quad (3)$$

where ε_m is the mechanical strain, ε is the total strain and ε_T is the thermal strain. We implemented these relations in a finite element code based on Bernoulli-Euler beam elements and conducted several thermal deformation analyses.

Numerical Conditions

In terms of the thermal history for the analysis, we gradually increased the temperature step-by-step from 0°C to 50°C at an increment of 1°C and then held the temperature at a steady state. Then, we applied the actual thermal history detected on the ETS-VIII as an input for the analysis, as shown in Fig. 8. The displacement evaluation point was defined at the centre and peripheral side of the upper radial member of each module. The spring force was also gradually increased step-by-step from 1 N to 233 N along with the temperature transition in the first phase, as shown in Fig. 9 (areas A-D are explained in Fig. 13). Then, we carried out thermal deformation analyses with and without controlling the spring force.

The analyses we carried out are summarized as follows.

- Case 0: original case, without any means of suppression
  (aims to confirm how the thermal deformation occurred in the 14-module model)

Thermal deformation suppressed using the following:

- Case 1: control spring forces uniformly in all modules
- Case 2: adjust the combined CTE of the structural members
- Case 3: adjust the combined CTE of the structural members and by then control spring forces differently in each module depending on the distances from the constraint point

Thermal Deformation Analysis

Case 0

According to the thermal deformation analysis of the original model without any means of suppression, displacements occurred in the direction normal to the reflector surface during thermal transition, as shown in Figs. 10 and 11. As shown in Table 1 and Fig. 12(a), these displacements occurred due to the combined CTE of the diagonal member; the combined CTE was three times greater than that of the lower radial member, which helped the member shrink. Furthermore, the upper radial member, with a negative CTE value, expanded when the temperature decreased. Therefore, the displacements occurred in a downward direction. A position further from the constraint point resulted in a greater centre side deformation due to the accumulation of displacements. In the farthest module, the displacements were approximately 20 mm. Moreover, the midpoint of the LDR was confirmed to deform by approximately 5 mm, which explains the phenomena actually observed on the ETS-VIII [4-6].

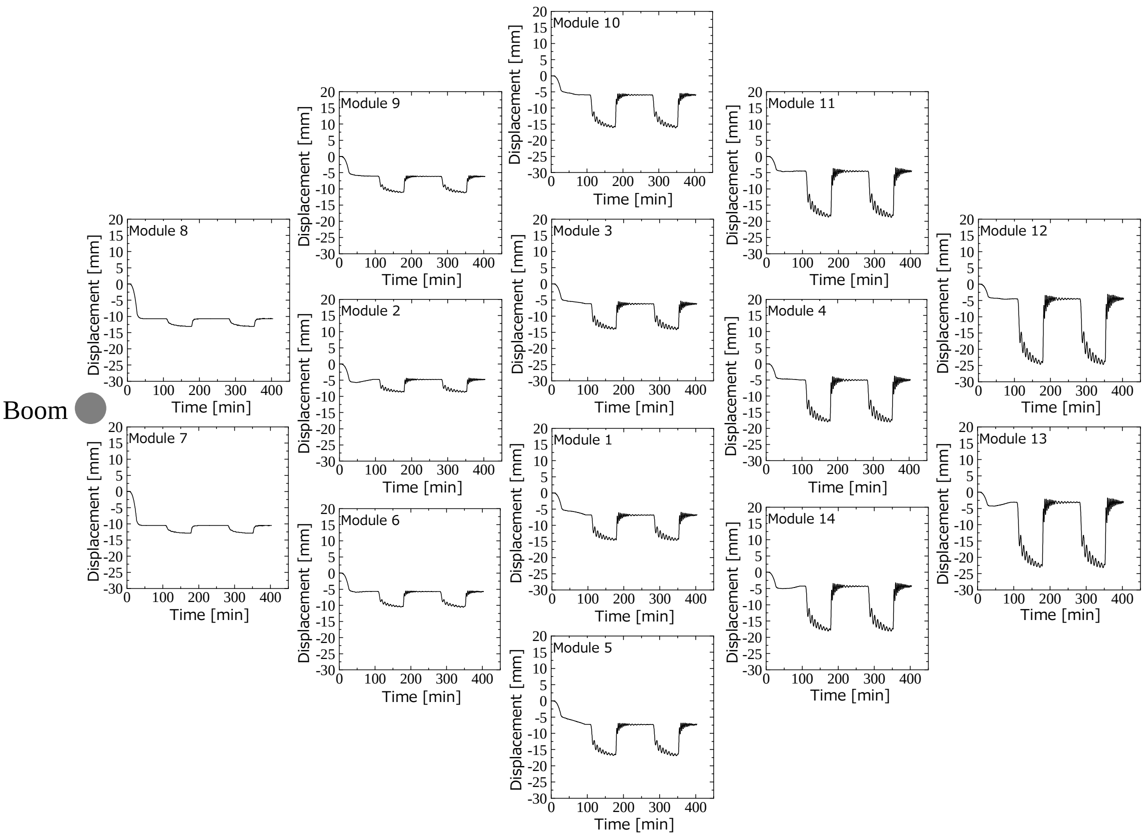

Fig. 10: Displacements occurred in a direction normal to the reflector surface on the centre side of the upper radial member in Case 0

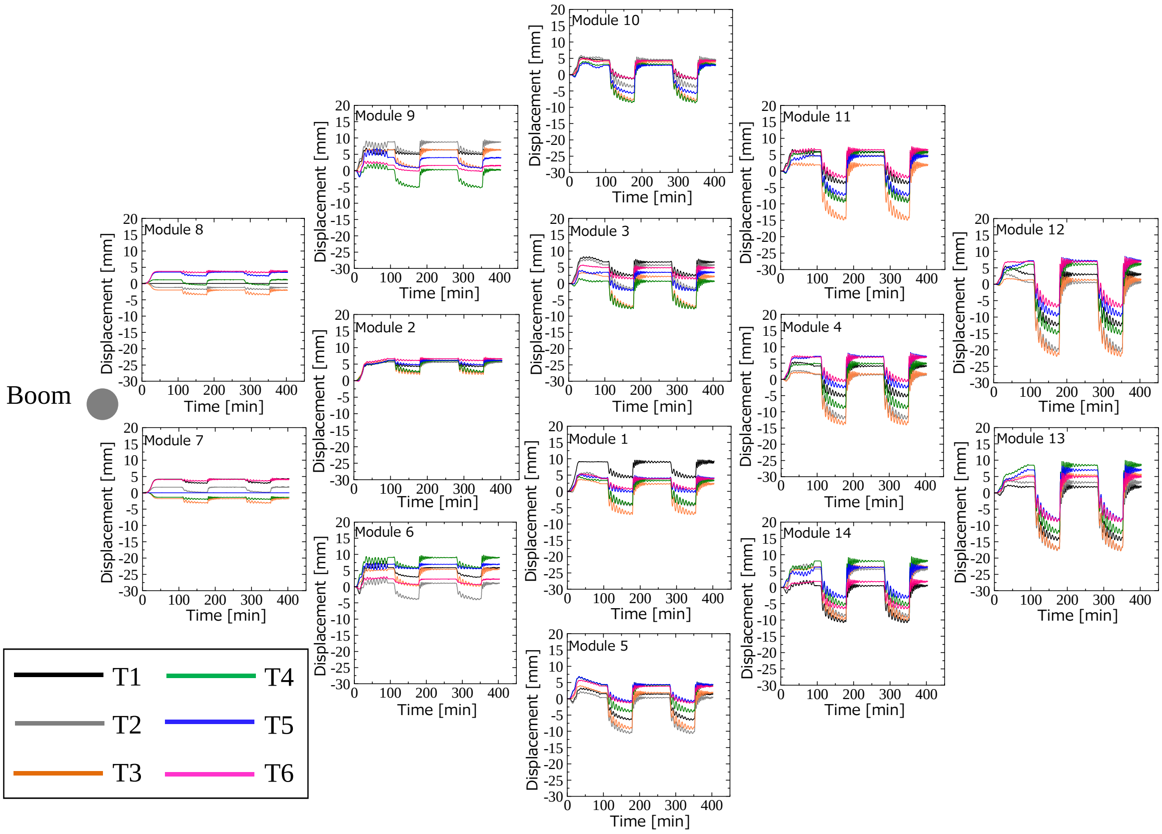

Fig. 11: Displacements occurred in a direction normal to the reflector surface on the peripheral side of the upper radial member in Case 0

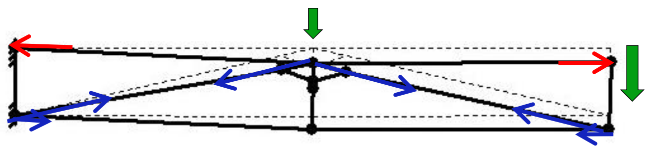

(a) Without control

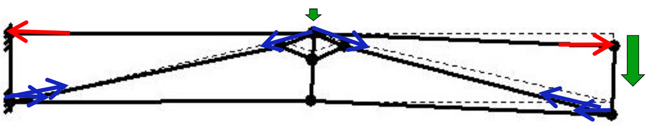

(b) With control

Broken line: Point T_A (50°C)
Solid line: Point T_B (-150°C)

Fig. 12: Schematic diagram of the thermal deformation due to a decrease in the temperature

Case 1

As a result of controlling spring forces uniformly in all modules as shown in Fig. 9(b), only the centre side of the upper radial member was suppressed successfully and we confirmed that this resulted in no suppression of the peripheral side of the upper radial member. The mechanism explaining this phenomenon is the following. As shown in Fig. 12(b), the compression force generated at the diagonal member was reduced, and the centre side of the upper radial member was lifted due to the spring force control. However, the upper radial member remained stretched due to thermal expansion, and the peripheral sides remained deformed in the downward direction.

Furthermore, this result has shown that the thermal deformation could be suppressed by distributing different spring forces in four areas depending on the distances from the constraint point, as shown in Fig. 13. Therefore, we attempted to suppress the thermal deformation, in Case 3, by controlling spring forces differently in each area.

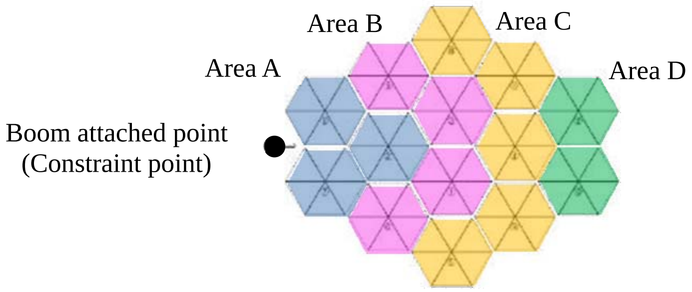

Fig. 13: Schematic diagram of the partitions used to control different spring forces

Table 2: Optimal combination of the combined CTE

	Material	Combined CTE (10-6/K)	
		Case 0	Case 2, Case 3
Upper radial member	CFRP	-0.182	-0.182
Lower radial member	CFRP	0.312	-0.005
Diagonal member	CFRP	0.948	0.948
Centre axis member	CFRP	3.490	3.490
Longitudinal member	CFRP	0.277	0.277
Joint member	Titanium alloy	8.800	8.800

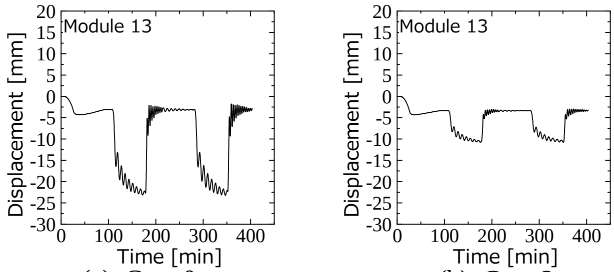

(a) Case 0 (b) Case 2

Fig. 14: Suppression effect at the centre side of the upper radial member

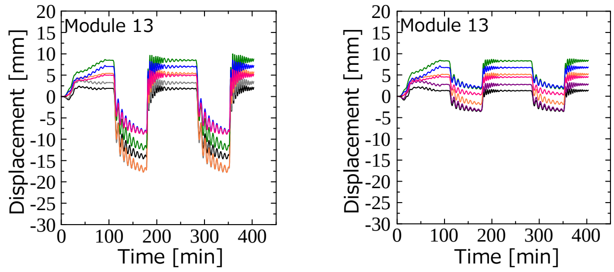

(a) Case 0 (b) Case 2

Fig. 15: Suppression effect at the peripheral side of the upper radial member

Case 2

The thermal deformation that occurred in the peripheral sides of upper radial member cannot be suppressed sufficiently by distributing different spring forces alone. Therefore, we attempted to suppress the thermal deformation that occurred in the peripheral sides of the upper radial member by adjusting the combined CTE of the structural members. We focused on the combined CTE of the upper radial member and the lower radial member. These CTE values have opposite signs. In other words, there is a possibility that the thermal deformation can be suppressed by an optimal combination of combined CTEs. Therefore, we carried out some parametric studies by changing the combined CTE of the lower radial member, and then the optimized combination was found and is shown in Table 2. As a result, this method resulted in some suppression effects at the centre and the peripheral side of the upper radial member, as shown in Figs. 14 and 15.

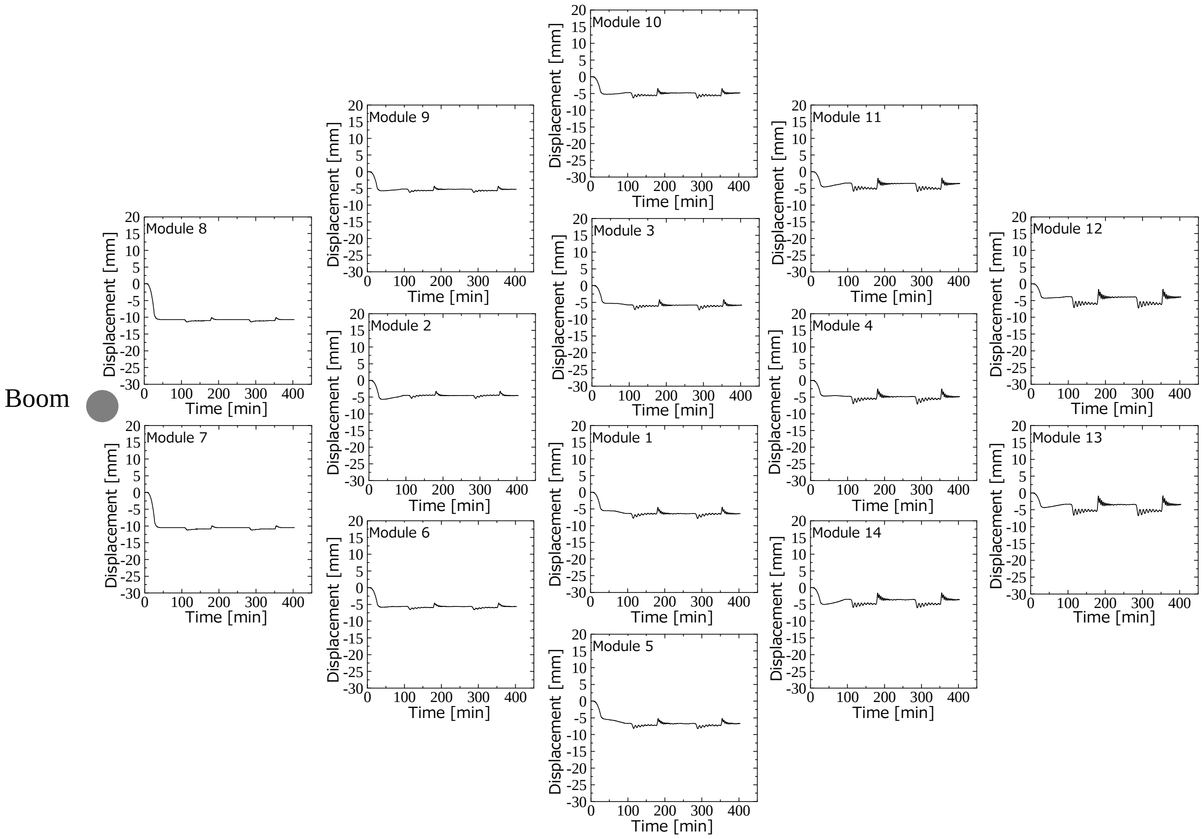

Fig. 16: Displacements occurred in direction normal to the reflector surface on the centre side of the upper radial member in Case 3

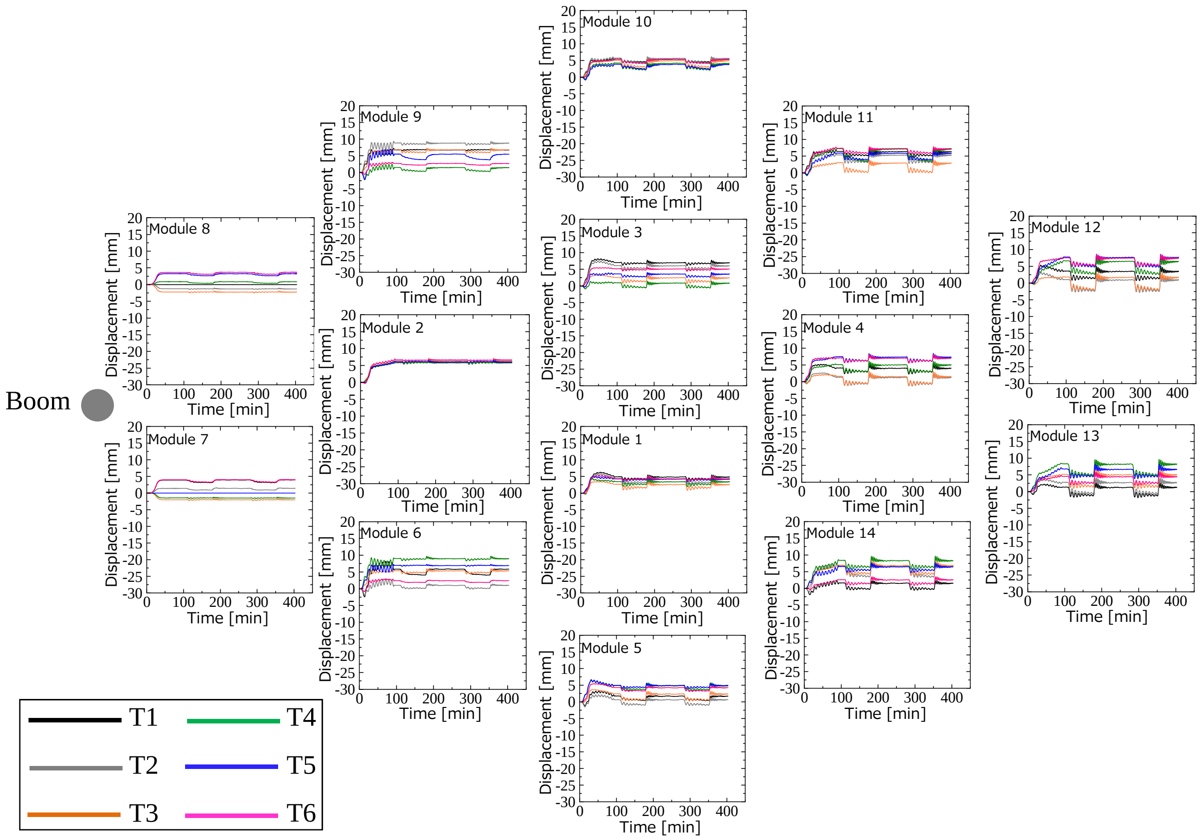

Fig. 17: Displacements occurred in a direction normal to the reflector surface on the peripheral side of the upper radial member in Case 3

Table 3: Displacements obtained for each module in each case

Area	Module No.	Evaluation point	Case 0 (mm)	Case 1 (mm)	Case 2 (mm)	Case 3 (mm)
A	8	Centre side	2.4	0.6	2.4	0.6
		Peripheral side	0.8	1.1	0.2	0.3
	2	Centre side	3.8	1.4	2.7	0.3
		Peripheral side	2.2	1.8	0.6	0.2
	7	Centre side	2.4	0.7	2.4	0.7
		Peripheral side	0.8	1.2	0.2	0.4
B	9	Centre side	5.0	3.0	3.0	0.4
		Peripheral side	3.2	3.2	0.9	0.8
	3	Centre side	7.7	4.9	3.8	0.4
		Peripheral side	6.2	5.3	1.9	0.9
	1	Centre side	7.5	4.7	3.7	0.1
		Peripheral side	6.1	5.2	1.7	0.8
	6	Centre side	4.7	2.9	2.8	0.3
		Peripheral side	3.1	3.1	0.6	0.7
C	10	Centre side	10.0	7.3	4.5	0.9
		Peripheral side	7.4	7.5	2.6	1.5
	11	Centre side	13.8	10.8	5.7	1.8
		Peripheral side	10.6	10.9	3.9	2.3
	4	Centre side	12.6	9.3	5.2	0.8
		Peripheral side	11.2	9.7	3.4	1.7
	14	Centre side	13.4	10.5	5.3	1.4
		Peripheral side	10.3	10.4	3.5	2.1
	5	Centre side	9.3	7.0	3.9	0.6
		Peripheral side	7.9	7.3	1.9	1.3
D	12	Centre side	19.6	15.9	7.4	2.4
		Peripheral side	15.5	15.9	5.7	3.2
	13	Centre side	19.5	15.8	7.2	2.2
		Peripheral side	15.3	15.8	5.5	3.0

Case 3

Based on the results of Case 1 and Case 2, we aimed to suppress these thermal deformations more effectively in Case 3 by adjusting the combined CTE of the structural members and by then controlling spring forces differently in four areas. As seen in Figs. 16 and 17, the thermal deformations are almost suppressed not only at the centre side of the upper radial member but also at the peripheral sides. The effect can be clearly seen in the obtained displacements, as shown in Table 3. The displacements in Case 3 were drastically reduced in all areas compared with the original case (Case 0). Particularly, the average maximum displacements were decreased from approximately 5mm (in Case 0) to 0.5 mm (in Case 3) at modules 1 and 3, which located at the centre of the LDR, where the electric field strength became the highest. These results indicate that the transition of the communication beam on the surface of the earth can be decreased to a range of 5 to 10 km.

Conclusions

A finite element model of the LDR was constructed, and a thermal deformation analysis was performed to investigate the deformation behaviour of the LDR during thermal transition. The displacements occurred in the direction normal to the reflector surface during thermal transition. Moreover, the midpoint of the LDR was confirmed to deform by approximately 5 mm, which explains the phenomena actually observed on the ETS-VIII.

Furthermore, we attempted to seek out a means to suppress the thermal deformation mechanically by adjusting the CTE of the structural members and by then controlling spring forces differently in four areas. As a consequence, the thermal deformations at every apex that support the antenna reflector were all suppressed at a high correction rate. These results indicate that the transition of the communication beam on the surface of the earth can be decreased to a range of 5 to 10 km.

References

1. Usui, M., Wakita, K.,Kondo, K., Thanh , L. T. T., Matsui, Y. and Isobe, D., “Suppression of thermal deformation of the large deployable reflector”, *Transactions of the Japan Society of Mechanical Engineers*, Series C, Vol.77, No.777, 2011, pp.2107–2119 (in Japanese).

2. Fujino, Y., Satoh, M. and Orikasa, M., “Beam variation of large-scale deployable antenna mounted on satellite in geostational orbit”, *Transactions of the Institute of Electronics, Information and Communication Engineers*, IEICE Technical Report, 2008, pp.15–18 (in Japanese).

3. Satoh, M., Orikasa, T., Fujino, Y., Kawasaki, K., Yamamoto, S., Miura, A. and Taira, S., “Beam direction variation of large-scale deployable reflector antenna on the satellite orbit”, *Transactions of the Institute of Electronics, Information and Communication Engineers*, IEICE Technical Report, 2010, pp.19–24 (in Japanese).

4. Satoh, M., Fujino, Y. and Orikasa, T., “Characterization of large-scale deployable antenna pattern equipped with engineering test satellite VIII on orbit”, *Transactions of the Institute of Electronics, Information and Communication Engineers*, IEICE Technical Report, Series B, Vol.J91-B, No.12, 2008, pp.1641–1643 (in Japanese).

5. Satoh, M., Orikasa, T., Fujino, Y., Orikasa, T., Kohata, H., Usui, M. and Yamasa, Y., “Beam direction shift of large-scale antenna on ETS-VIII during eclipse”, *Proceedings of the General Conference of the Institute of Electronics, Information and Communication Engineers*, Series 1, 2009, pp.337 (in Japanese).

6. Usui, M. and Isobe, D., “Antenna pattern during earth eclipse and suppression of thermal deformation of the large deployable reflector of the ETS-VIII”, *Proceedings of the Communications Society Conference of the Institute of Electronics, Information and Communication Engineers*, Series 1, 2011, pp.301 (in Japanese).